

# Mesh Stiffness Variation Instabilities in Two-Stage Gear Systems

Jian Lin  
Mem. ASME

John Deere Product Engineering Center,  
Waterloo, IA 50704-8000

Robert G. Parker

Mem. ASME Associate Professor,  
Department of Mechanical Engineering,  
The Ohio State University,  
206 W. 18th Ave,  
Columbus, OH 43210  
e-mail: parker.242@osu.edu

*Mesh stiffness variation, the change in stiffness of meshing teeth as the number of teeth in contact changes, causes parametric instabilities and severe vibration in gear systems. The operating conditions leading to parametric instability are investigated for two-stage gear chains, including idler gear and countershaft configurations. Interactions between the stiffness variations at the two meshes are examined. Primary, secondary, and combination instabilities are studied. The effects of mesh stiffness parameters, including stiffness variation amplitudes, mesh frequencies, contact ratios, and mesh phasing, on these instabilities are analytically identified. For mesh stiffness variation with rectangular waveforms, simple design formulas are derived to control the instability regions by adjusting the contact ratios and mesh phasing. The analytical results are compared to numerical solutions. [DOI: 10.1115/1.1424889]*

## 1 Introduction

Vibration and noise reduction is a major concern in powertrain and gearing applications. A primary source of gear vibration and noise is the dynamic excitation from the changing stiffness of the meshing teeth. The mesh stiffness associated with elastic tooth bending varies as the number of teeth in contact changes. The parametric excitation from the time-varying mesh stiffness causes instability and severe vibration under certain operating conditions. Experiments [1,2] have demonstrated the large amplitude vibration induced by parametric instability where the gear mesh frequency equals twice the natural frequency (primary instability) or the natural frequency (secondary instability). Furthermore, mesh stiffness variation directly affects tooth deflections and transmission error. To a large extent, gear resonance excited by harmonics of transmission error arises fundamentally from mesh stiffness variation [3,4,5,6]. Therefore, determination of operating conditions of parametric instability and identification of design parameters that minimize their occurrence are crucial to the design of quiet gear chains.

Parametric instability in general dynamic systems has been studied extensively. Literature reviews of parametrically excited systems can be found in the work of Ibrahim and Barr [7] and Nayfeh and Mook [8]. For a single pair of gears, Bollinger and Harker [9] determined instability conditions using a single degree-of-freedom Mathieu equation model. Benton and Seireg [1] experimentally simulated instabilities under parametric excitations and demonstrated the damage of parametric instability on gear teeth. Other researchers [3–5,10–13] also investigated gear parametric instability for single mesh systems. When forcing excitation and clearance nonlinearity interact with parametric excitation, complicated phenomena are observed in single mesh gear models [3–5]. For gear systems having multiple degrees-of-freedom, it is surprising to find little work on parametric instability in the published literature. Tordion and Gauvin [14] and Benton and Seireg [15] studied the same two-stage gear systems [Fig. 1(a)] but reached conflicting conclusions on the conditions causing instability. Furthermore, their results do not agree with those obtained herein by analytical and numerical methods. In short, the existing analysis on parametric instability is scarce, inconsistent, and incomplete for multi-mesh gear systems.

The objective of this study is to systematically analyze the op-

erating conditions leading to parametric instability in two-mesh, multi-gear systems (Fig. 1). The two meshes can have different mesh frequencies, amplitudes of mesh stiffness variation, contact ratios, and mesh phasing. The study applies a perturbation method to determine instability conditions and numerically verifies the results. The effects of contact ratios and mesh phasing on the stability boundaries are expressed in simple formulas that allow designers to suppress particular instabilities by properly selecting parameters. This analysis reveals errors in previous analyses of the same system [14,15] and, in contrast with these works, yields conclusions consistent with numerical methods. The two-stage gear systems and mesh stiffness modeling are introduced first. The instability conditions are then derived. Three cases having various mesh frequency relationships and amplitudes of mesh stiffness variation are studied separately. Finally, the analytical and numerical results are compared with two previous studies through a benchmark example, clarifying major differences in these prior works.

## 2 Two-Mesh Gear System Models

Two-stage gear trains have three-gear and four-gear configurations (Fig. 1). Only rotational vibrations  $\theta_1$ ,  $\theta_2$ ,  $\theta_3$  relative to the rigid body gear rotations are considered. The input shaft has torsional stiffness  $k_{L0}$  and is anchored to a body rotating at constant speed (e.g., drive motor). The intermediate shaft connecting gears 2 and 4 is assumed rigid, which is reasonable for the typical case of gears 2 and 4 being immediately adjacent or made from one piece. The tooth meshes are modeled as linear springs with stiffnesses  $k_{L1}$ ,  $k_{L2}$ . Contact loss due to parametric instability, which is critical for calculation of vibration amplitude, is not the focus of the work. The gears have base radii  $r_i$ ,  $i = 1, 2, 3, 4$ . The equivalent masses are  $m_1 = I_1/r_1^2$ ,  $m_2 = I_2/r_2^2$ , and  $m_3 = vI_3/r_3^2$ , where  $I_i$  are the moments of inertia of the gears and their connected shafts,  $v = r_4/r_2$  for four-gear trains, and  $v = 1$  for three-gear chains. The equivalent stiffnesses are  $k_0 = k_{L0}/r_1^2$ ,  $k_1 = k_{L1}$ , and  $k_2 = v^2 k_{L2}$ . The shaft/gear rotations are measured by the base radius deflections  $x_1 = \theta_1 r_1$ ,  $x_2 = \theta_2 r_2$ , and  $x_3 = \theta_3 r_3/v$ . The system stability is governed by the free vibration equation

$$\mathbf{M}\ddot{\mathbf{q}} + [\mathbf{K}_0 + \mathbf{K}_v(t)]\mathbf{q} = 0 \quad (1)$$

where  $\mathbf{q} = [x_1, x_2, x_3]^T$ .  $\mathbf{M} = \text{diag}(m_1, m_2, m_3)$  is the inertia matrix. The stiffness matrix is represented by a mean value  $\mathbf{K}_0$  and a variational part  $\mathbf{K}_v(t)$  as

Contributed by the Technical Committee on Vibration and Sound for publication in the JOURNAL OF VIBRATION AND ACOUSTICS. Manuscript received August 2000; Revised September 2001. Associate Editor: L. A. Bergman.

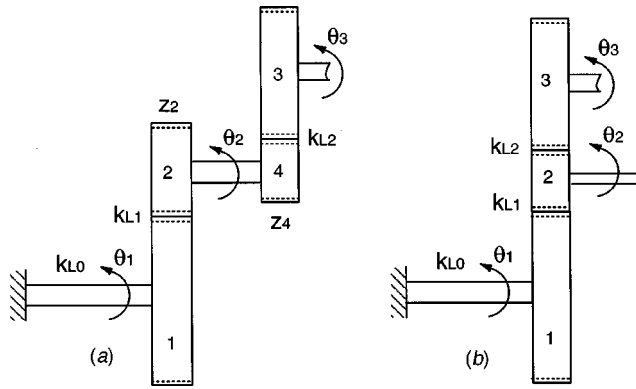


**Fig. 1** Two-stage gear system with (a) four gears and (b) three gears.  $k_{L1}$ ,  $k_{L2}$  denote mesh stiffnesses and  $Z_2, Z_4$  denote number of gear teeth.  $k_{L0}$  is the torsional stiffness of the anchored shaft.

$$\mathbf{K}_0 = \begin{bmatrix} k_{g1} + k_0 & k_{g1} & 0 \\ k_{g1} & k_{g1} + k_{g2} & k_{g2} \\ 0 & k_{g2} & k_{g2} \end{bmatrix}$$

$$\mathbf{K}_v(t) = \begin{bmatrix} k_{v1} & k_{v1} & 0 \\ k_{v1} & k_{v1} + k_{v2} & k_{v2} \\ 0 & k_{v2} & k_{v2} \end{bmatrix} \quad (2)$$

where  $k_{gi}$  and  $k_{vi}(t)$  are the mean and time-varying components of the mesh stiffnesses,  $k_i(t) = k_{gi} + k_{vi}(t)$  (Fig. 2).

The variational parts  $k_{vi}(t)$  are periodic at the mesh frequency  $\Omega_i$  and expressed in Fourier series as

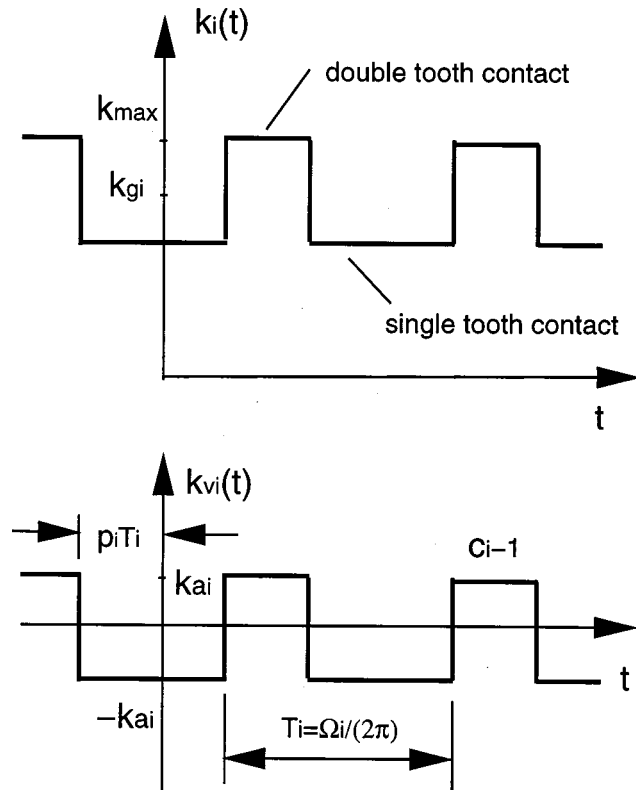


**Fig. 2** Modeling of mesh stiffnesses  $k_i(t) = k_{gi} + k_{vi}(t)$ .  $c_i$  are contact ratios,  $k_{gi}$  are average mesh stiffnesses, and  $p_i T_i$  are phasing angles.

$$k_{vi}(t) = 2k_{ai} \sum_{s=1}^{\infty} (a_i^{(s)} \sin s\Omega_i t + b_i^{(s)} \cos s\Omega_i t), \quad i=1,2 \quad (3)$$

where  $2k_{ai}$  is the peak-to-peak amplitude of  $k_{vi}$  (Fig. 2). The mesh frequencies  $\Omega_1$  and  $\Omega_2$  are related by  $\Omega_1 = R\Omega_2$ , where  $R = Z_2/Z_4$  and  $Z_2, Z_4$  are the numbers of teeth on gears 2 and 4 [Fig. 1(a)]. Note  $R=1$ ,  $\Omega_1 = \Omega_2$  for three-gear systems [Fig. 1(b)]. Mesh stiffness variation is obtained through measurement, calculation, or simple specification (e.g., sinusoidal or rectangular wave). For spur gears, rectangular waves are often used to approximate the mesh stiffness alternating between  $n$  and  $n+1$  pairs of teeth in contact [16]. In this study, the  $k_{vi}$  are specified as rectangular waves with variational amplitudes  $k_{ai}$ , periods  $T_i = \Omega_i/2\pi$ , contact ratios  $c_i$ , and phasing angles  $p_i T_i$  [Fig. 2(b)]. Thus,

$$a_i^{(s)} = -\frac{2}{s\pi} \sin[s\pi(c_i - 2p_i)] \sin(s\pi c_i),$$

$$b_i^{(s)} = -\frac{2}{s\pi} \cos[s\pi(c_i - 2p_i)] \sin(s\pi c_i) \quad (4)$$

in (3) for  $s=1,2,\dots$ . Without loss of generality, one can specify  $p_1=0, p_2=h$  ( $h$  is called mesh phasing). In practice, the first three or four Fourier terms reasonably approximate the mesh stiffness variation.

For the time-invariant case, the eigenvalue problem associated with (1) is

$$\mathbf{K}_0 \phi_i = \omega_i^2 \mathbf{M} \phi_i \quad (5)$$

where  $\omega_i$  are the natural frequencies. The vibration modes  $\phi_i$  are normalized as  $\Phi^T \mathbf{M} \Phi = \mathbf{I}$  with  $\Phi = [\phi_1, \phi_2, \phi_3]$ . Applying the modal transformation  $\mathbf{q} = \Phi \mathbf{u}$  and using (3), Eq. (1) becomes

$$\ddot{u}_n + \omega_n^2 u_n + \sum_{r=1}^3 \sum_{s=1}^{\infty} [2\varepsilon_1 (D_{nr}^{(s)} \sin s\Omega_1 t + E_{nr}^{(s)} \cos s\Omega_1 t) + 2\varepsilon_2 (F_{nr}^{(s)} \sin s\Omega_2 t + G_{nr}^{(s)} \cos s\Omega_2 t)] u_r = 0, \quad n=1,2,3 \quad (6)$$

where  $\varepsilon_i = k_{ai}/k_{gi}$ ,  $i=1,2$  and  $D_{nr}^{(s)}, E_{nr}^{(s)}, F_{nr}^{(s)}, G_{nr}^{(s)}$  are elements of the matrices

$$\mathbf{D}^{(s)} = k_{g1} \Phi^T \begin{bmatrix} a_1^s & a_1^s & 0 \\ a_1^s & a_1^s & 0 \\ 0 & 0 & 0 \end{bmatrix} \Phi \quad \mathbf{E}^{(s)} = k_{g1} \Phi^T \begin{bmatrix} 0 & 0 & 0 \\ 0 & b_1^s & b_1^s \\ 0 & b_1^s & b_1^s \end{bmatrix} \Phi$$

$$\mathbf{F}^{(s)} = k_{g2} \Phi^T \begin{bmatrix} a_2^s & a_2^s & 0 \\ a_2^s & a_2^s & 0 \\ 0 & 0 & 0 \end{bmatrix} \Phi \quad \mathbf{G}^{(s)} = k_{g2} \Phi^T \begin{bmatrix} 0 & 0 & 0 \\ 0 & b_2^s & b_2^s \\ 0 & b_2^s & b_2^s \end{bmatrix} \Phi \quad (7)$$

Equation (6) is a set of coupled Hill's equations subjected to multi-frequency parametric excitations from two gear meshes.

Parametric excitations give rise to instabilities when harmonics of the excitation frequencies are close to particular combinations of the natural frequencies. Three types of instability are of most interest: (1) primary instability  $\Omega_i \approx 2\omega_p$ , (2) secondary instability  $\Omega_i \approx \omega_p$ , and (3) combination instability  $\Omega_i \approx \omega_p + \omega_q$ , where  $\omega_p, \omega_q$  are different natural frequencies. Plots of the excitation (mesh) frequency  $\Omega_i$  versus the amplitude of the stiffness variation  $k_{ai}$  illustrate the instability regions under operating conditions (for example, Fig. 3). Perturbation methods [8,17,18] are used in this study to determine the boundaries separating the stable and unstable regions. Floquet theory and numerical integration are used to validate the analytical findings.

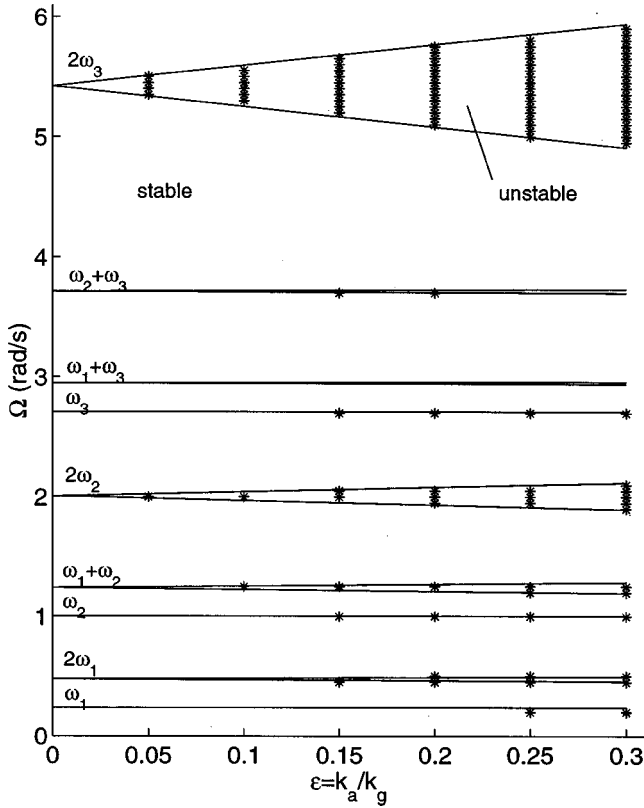


**Fig. 3** Instabilities regions when  $\Omega_1 = \Omega_2 = \Omega$ ,  $\varepsilon_1 = \varepsilon_2 = \varepsilon$ ; — analytical solution;\*\*\* numerical solution. The parameters are from Table 1 and  $c_1 = c_2 = 1.5$ ,  $h = 0$ .

### 3 Conditions of Parametric Instability

Parametric instability depends on the frequency, amplitude, and shape of the parametric excitations. In gear systems, these factors are directly associated with the operating speed and gear design parameters such as contact ratio, facewidth, diametral pitch, pressure angle, material properties, and so on. The corresponding model parameters are the stiffness variation amplitudes  $k_{a1}$ ,  $k_{a2}$ , mesh frequencies  $\Omega_1, \Omega_2$ , contact ratios  $c_1, c_2$ , and mesh phasing  $h$ .

In practice, the variation amplitudes  $k_{ai}$  are small compared to the average mesh stiffnesses  $k_{gi}$  ( $\varepsilon_i < 0.5$  according to a simple approximation [16]). At this point,  $\varepsilon_1 = \varepsilon_2 = \varepsilon$  is specified; the case of  $\varepsilon_1 \neq \varepsilon_2$  is discussed later. Using the method of multiple scales, the solution of Eq. (6) is expressed as

$$u_n = u_{n0}(t, \tau) + \varepsilon u_{n1}(t, \tau) + \dots \quad n = 1, 2, 3 \quad (8)$$

where  $\tau = \varepsilon t$ . Substituting Eqs. (8) into (6) and collecting terms of the same power in  $\varepsilon$  yields

$$\ddot{u}_{n0} + \omega_n^2 u_{n0} = 0 \quad n = 1, 2, 3 \quad (9)$$

$$\ddot{u}_{n1} + \omega_n^2 u_{n1} = -2 \frac{\partial u_{n0}}{\partial \tau} - 2 \sum_{r=1}^3 \sum_{s=1}^{\infty} [D_{nr}^{(s)} \sin s \Omega_1 t + E_{nr}^{(s)} \cos s \Omega_1 t + F_{nr}^{(s)} \sin s \Omega_2 t + G_{nr}^{(s)} \cos s \Omega_2 t] u_{r1} \quad (10)$$

The general solutions of Eq. (9) are

$$u_{n0} = A_n(\tau) e^{i \omega_n t} + c.c. \quad n = 1, 2, 3 \quad (11)$$

The symbol  $c.c.$  represents the complex conjugate of preceding terms. Substitution of Eq. (11) into (10) yields

$$\begin{aligned} \ddot{u}_{n1} + \omega_n^2 u_{n1} = & -2i \omega_n e^{i \omega_n t} \frac{\partial A_n}{\partial \tau} - \sum_{r=1}^3 \sum_{s=1}^{\infty} A_r \{ D_{nr}^{(s)} [e^{i(\omega_n + s \Omega_1)t} \\ & + e^{i(\omega_n - s \Omega_1)t}] - i E_{nr}^{(s)} [e^{i(\omega_n + s \Omega_1)t} - e^{i(\omega_n - s \Omega_1)t}] \\ & + F_{nr}^{(s)} [e^{i(\omega_n + s \Omega_2)t} + e^{i(\omega_n - s \Omega_2)t}] - i G_{nr}^{(s)} [e^{i(\omega_n + s \Omega_2)t} \\ & - e^{i(\omega_n - s \Omega_2)t}] \} + c.c. \quad n = 1, 2, 3 \quad (12) \end{aligned}$$

Three different mesh conditions are examined.

#### 3.1 Three-Gear Systems: Equal Mesh Stiffness Variations.

In three-gear systems [Fig. 1(b)], the two meshes have the same mesh frequencies  $\Omega_1 = \Omega_2 = \Omega$ . We consider the case where the gear facewidths and material properties, which primarily determine mesh stiffness for a given number of teeth in contact, are such that the amplitudes of mesh stiffness variation are the same at the two meshes ( $\varepsilon_1 = \varepsilon_2 = \varepsilon$ ). The contact ratios and mesh phasing are allowed to differ between the two meshes, however. In practice, the contact ratios are changed using center distance, diametral pitch, pressure angle, tooth addendum, and other parameters. The mesh phasing depends on the layout of the gears and the numbers of teeth.

The parametric instability when  $s\Omega$  is close to  $\omega_p + \omega_q$  is considered. Let  $s\Omega = \omega_p + \omega_q + \sigma\varepsilon$ , where  $\sigma$  is a detuning parameter to be determined. Elimination of terms leading to unbounded response in Eq. (12) requires

$$2i \omega_p \partial A_p / \partial \tau + \bar{A}_q [(D_{pq}^{(s)} + F_{pq}^{(s)}) + i(E_{pq}^{(s)} + G_{pq}^{(s)})] e^{i\sigma\tau} = 0 \quad (13)$$

$$2i \omega_q \partial A_q / \partial \tau + \bar{A}_p [(D_{qp}^{(s)} + F_{qp}^{(s)}) + i(E_{qp}^{(s)} + G_{qp}^{(s)})] e^{i\sigma\tau} = 0 \quad (14)$$

The nontrivial solutions of Eq. (13) and (14) have the form

$$A_p = a_p e^{-i\lambda\tau}, \quad A_q = a_q e^{-i(\lambda + \sigma)\tau} \quad (15)$$

where  $a_p, a_q$  are complex constants and the  $\lambda$  below are roots of the associated characteristic equation

$$\lambda = -\frac{1}{2} [\sigma \pm (\sigma^2 - \Lambda_{pq}^{(s)})^{1/2}],$$

$$\Lambda_{pq}^{(s)} = \frac{1}{\omega_p \omega_q} [(D_{pq}^{(s)} + F_{pq}^{(s)})^2 + (E_{pq}^{(s)} + G_{pq}^{(s)})^2] \quad (16)$$

From Eq. (15) and (16),  $A_p$  and  $A_q$  are bounded when  $\sigma^2 > \Lambda_{pq}^{(s)}$  and unbounded when  $\sigma^2 < \Lambda_{pq}^{(s)}$ . Thus, the boundaries of the instability regions are

$$\Omega = \frac{1}{s} (\omega_p + \omega_q \pm \varepsilon \sqrt{\Lambda_{pq}^{(s)}}) \quad (17)$$

For single mode instabilities ( $p = q$ ), Eq. (17) becomes

$$\Omega = \frac{2\omega_p}{s} \pm \frac{\varepsilon}{s\omega_p} [(D_{pp}^{(s)} + F_{pp}^{(s)})^2 + (E_{pp}^{(s)} + G_{pp}^{(s)})^2]^{1/2}, \quad s = 1, 2, \dots \quad (18)$$

As an example, Fig. 3 shows the boundaries for primary ( $s = 1$ ), secondary ( $s = 2$ ), and combination ( $p \neq q, s = 1$ ) instabilities. The parameters are given in Table 1 and  $c_1 = c_2 = 1.5$ ,  $h = 0$ . Floquet theory [8] is used to determine the actual instability regions denoted by \* in the figures. The method to compute the fundamental matrix and numerically determine stability are given in [19]. The first-order approximations from Eq. (17) agree well with the numerical solution, even when  $\varepsilon$  is not small. In Fig. 3, the instability region around  $\Omega \approx 2\omega_3$  is much larger than that of the primary instabilities around  $2\omega_1$  and  $2\omega_2$ . This is explained by examining the vibration modes. From Eq. (17), the primary instability boundary slopes are governed by  $\sqrt{\Lambda_{pp}^{(s)}}$ . Expansion of **D**, **E**, **F**, **G** in Eq. (7) yields the diagonal terms

**Table 1 Parameters of an example system in Fig. 2**

Inertia	$m_1=1, m_2=0.3, m_3=4.0$
Average mesh stiffness	$k_{g1}=k_{g2}=1$
Shaft stiffness	$k_0=0.5$
Contact ratio	$1 \leq c_1, c_2 \leq 2$
Mesh phasing	$p_1=0, 0 \leq p_2=h \leq 1$
Variational amplitude	$0 \leq k_{a1}, k_{a2} \leq 0.5$

$$\begin{aligned}
 D_{pp}^{(s)} &= k_{g1}(\phi_{1p} + \phi_{2p})^2 a_1^{(s)}, & F_{pp}^{(s)} &= K_{g2}(\phi_{2p} + \phi_{3p})^2 a_2^{(s)} \\
 E_{pp}^{(s)} &= k_{g1}(\phi_{1p} + \phi_{2p})^2 b_1^{(s)}, & G_{pp}^{(s)} &= k_{g2}(\phi_{2p} + \phi_{3p})^2 b_2^{(s)}
 \end{aligned}
 \tag{19}$$

where  $\phi_{1p}, \phi_{2p}, \phi_{3p}$  are the element rotations in mode  $\phi_p$ .  $\delta_{1p} = \phi_{1p} + \phi_{2p}$  is the relative tooth deflection of the first mesh in mode  $\phi_p$ . Similarly,  $\delta_{2p} = \phi_{2p} + \phi_{3p}$  represents the modal deflection in the second mesh. For the primary instability boundary around  $2\omega_p$ , insertion of Eq. (19) into (16) yields

$$\begin{aligned}
 \Lambda_{pp}^{(1)} &= [(k_{g1}\delta_{1p}^2 a_1^{(1)} + k_{g2}\delta_{2p}^2 a_2^{(1)})^2 \\
 &\quad + (k_{g1}\delta_{1p}^2 b_1^{(1)} + k_{g2}\delta_{2p}^2 b_2^{(1)})^2] / \omega_p^2
 \end{aligned}
 \tag{20}$$

The mesh deflections  $\delta_1, \delta_2$  in each mode can be observed from the mode shapes (Fig. 4). The two meshes in  $\phi_1$  are both in phase and have smaller  $\delta_1, \delta_2$  than those of  $\phi_3$ , where the two meshes are both out of phase. Thus,  $\Lambda_{33}^{(1)} > \Lambda_{11}^{(1)}$  and the instability boundaries around  $2\omega_3$  have larger slope than those around  $2\omega_1$ . Mode  $\phi_2$  has one mesh in phase and the other out of phase, so the size

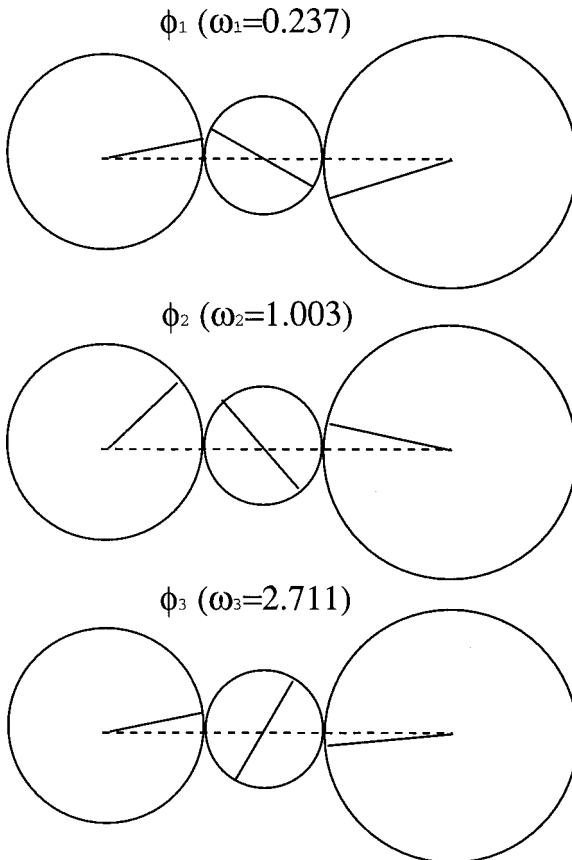


**Fig. 4 Vibration modes for the time-invariant system with parameters in Table 1**

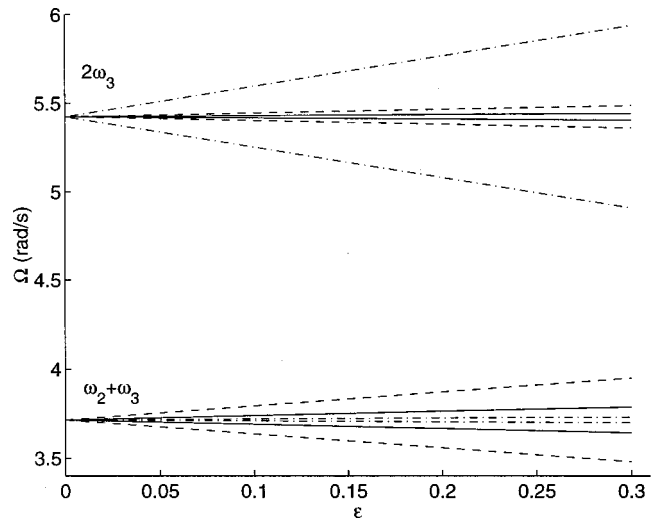


**Fig. 5 Comparison of instability regions for various contact ratios and mesh phasing. The parameters are in Table 1. --- $c_1=c_2=1.5, h=0.5$ ; - $c_1=1.1, c_2=1.9, h=0.9$ ; .....  $c_1=c_2=1.5, h=0$ .**

of its primary instability regions is between that of  $\phi_1$  and  $\phi_3$  ( $\Lambda_{33}^{(1)} > \Lambda_{22}^{(1)} > \Lambda_{11}^{(1)}$ ). In addition, the mesh deflections in a vibration mode are related to the modal strain energy  $U_1 = k_1 \delta_1^2 / 2$ ,  $U_2 = k_2 \delta_2^2 / 2$ . Examination of Eq. (20) shows that vibration modes with more strain energy in the meshes have larger instability regions and are more susceptible to parametric excitations. The above results apply for mesh stiffness variations of arbitrary shape.

For mesh stiffnesses having rectangular waveforms, one can clearly identify the effects of contact ratios and mesh phasing on the instability regions. Use of Eq. (4) in (20) yields

$$\begin{aligned}
 \Lambda_{pp}^{(1)} &= [k_{g1}^2 \delta_{1p}^4 \sin^2(c_1 \pi) + k_{g2}^2 \delta_{2p}^4 \sin^2(c_2 \pi) \\
 &\quad + 2k_{g1}k_{g2}\delta_{1p}^2\delta_{2p}^2 \sin(c_1 \pi)\sin(c_2 \pi)\cos(c_1 - c_2 + 2h)\pi] \\
 &\quad \times \left(\frac{2}{\pi\omega_p}\right)^2
 \end{aligned}
 \tag{21}$$

The minimum value  $\Lambda_{pp}^{(1)} = 0$  is obtained when  $\sin c_1 \pi = \sin c_2 \pi = 0$  and the unstable region vanishes. This is achieved for integer contact ratios  $c_1, c_2$  where the number of tooth pairs in contact remains constant and mesh stiffnesses are time-invariant. For given, non-integer  $c_{1,2}$  between 1 and 2,  $\Lambda_{pp}^{(1)}$  is minimized by setting  $\cos(c_1 - c_2 + 2h)\pi = -1$  or  $c_1 - c_2 + 2h = \pm 1, 3$ . By properly choosing the contact ratios and mesh phasing, the parametric instability regions can be dramatically reduced. Figure 5 compares the instability regions for three cases. The most severe condition for primary instabilities (dash-dot lines) is  $c_1 = c_2 = 1.5$  and  $h = 0$ , which maximizes  $\Lambda_{pp}^{(1)}$  in (21). This condition is markedly improved by changing the phasing  $h = 0.5$  so that  $c_1 - c_2 + 2h = 1$  (dashed lines). When the contact ratios are close to integers (solid lines,  $c_1 = 1.1, c_2 = 1.9, h = 0.9$ ), the primary instability region becomes even smaller.

For secondary instabilities ( $s = 2$ ), similar analysis yields

$$\begin{aligned}
 \Lambda_{pp}^{(2)} &= [k_{g1}^2 \delta_{1p}^4 \sin^2(2c_1 \pi) + k_{g2}^2 \delta_{2p}^4 \sin^2(2c_2 \pi) \\
 &\quad + 2k_{g1}k_{g2}\delta_{1p}^2\delta_{2p}^2 \sin(2c_1 \pi)\sin(2c_2 \pi) \\
 &\quad \times \cos 2(c_1 - c_2 + 2h)\pi] \left(\frac{1}{\pi\omega_p}\right)^2
 \end{aligned}
 \tag{22}$$

Maximum  $\Lambda_{pp}^{(2)} = (k_{g1}\delta_{1p}^2 + k_{g2}\delta_{2p}^2)^2$  occurs when  $\sin(2c_1\pi)\sin(2c_2\pi)\cos 2(c_1 - c_2 + 2h)\pi = 1$ . For  $1 \leq c_{1,2} \leq 2$  and  $0 \leq h < 1$ , the conditions for maximal secondary instability regions are  $c_1, c_2 = \{1.25, 1.75\}$  and  $h = 0$ . The secondary instability regions vanish for  $\sin 2c_1\pi = \sin 2c_2\pi = 0$  or  $c_1, c_2 = \{1, 1.5, 2\}$ . As a second choice, setting  $\cos 2(c_1 - c_2 + 2h)\pi = \pm 1$  with the sign opposite to  $\sin(2c_1\pi)\sin(2c_2\pi)$  also reduces these instabilities, that is,  $|c_1 - c_2 + 2h| = \{0.5, 1.5\}$  when  $c_1, c_2$  are both below or above 1.5, and  $|c_1 - c_2 + 2h| = \{0, 1, 2\}$  for other  $c_1, c_2$ .

For combination instabilities ( $p \neq q, s = 1$ ),

$$\Lambda_{pq}^{(1)} = [k_{g1}^2\delta_{1p}^2\delta_{1q}^2\sin^2(c_1\pi) + k_{g2}^2\delta_{2p}^2\delta_{2q}^2\sin^2(c_2\pi) + 2k_{g1}k_{g2}\delta_{1p}\delta_{2p}\delta_{1q}\delta_{2q}\sin(c_1\pi)\sin(c_2\pi)\cos(c_1 - c_2 + 2h)\pi] \left( \frac{4}{\pi^2\omega_p\omega_q} \right) \quad (23)$$

Depending on the sign of the product  $\delta_{1p}\delta_{2p}\delta_{1q}\delta_{2q}$ , the extreme regions of a combination instability can be achieved by adjusting  $c_1, c_2$ , and  $c_1 - c_2 + 2h$ .

Unfortunately, the primary, secondary, and combination instability regions cannot be minimized at the same time. The conditions reducing the primary instability regions (dashed lines, Fig. 5) result in large combination instability regions, and *vice versa* (dash-dot lines). Depending on specific applications, a trade-off may be made to reduce multiple instability regions, though none are true minima (solid lines). Adjusting contact ratios and mesh phasing is clearly an effective means to minimize instability regions and avoid resonances under operating conditions.

### 3.2 Four-Gear Systems: Equal Mesh Stiffness Variations.

Two-stage countershaft systems [Fig. 1(a)] have two different mesh frequencies  $\Omega_1 = R\Omega_2$ , which means more instability regions than three-gear systems. We consider the case where the gear facewidth and material are such that the mesh stiffness amplitudes are identical at the two meshes ( $\varepsilon_1 = \varepsilon_2 = \varepsilon$ ), although the contact ratios and phasing are not restricted. Depending on the ratio  $R = Z_2/Z_4$ , the parametric instability regions associated with  $\Omega_1$  and  $\Omega_2$  may overlap each other. For  $R = m/j$  ( $m, j$  are integers), the  $s = j$  instabilities (single mode and combination) of  $\Omega_1$  and the  $s = m$  instabilities of  $\Omega_2$  occur simultaneously. Because their instability regions are typically the largest, the interactions involving either  $m$  or  $j = 1$  are of most interest.

When  $R \neq m, 1/m$  for integer  $m$ , the  $s = 1$  instabilities from one mesh decouple from the  $s = m$  instabilities of the other mesh. In this case, instability occurs when  $s\Omega_1$  or  $s\Omega_2$  is close to  $\omega_p + \omega_q$ , but these instability boundaries can be calculated independently. For  $s\Omega_1 = \omega_p + \omega_q + \varepsilon\sigma_1$ , the terms leading to unbounded response in Eq. (12) are eliminated for

$$2i\omega_p\partial A_p/\partial\tau + \bar{A}_q(D_{pq}^{(s)} + iE_{pq}^{(s)})e^{i\sigma_1\tau} = 0 \quad (24)$$

$$2i\omega_q\partial A_q/\partial\tau + \bar{A}_p(D_{qp}^{(s)} + iE_{qp}^{(s)})e^{i\sigma_1\tau} = 0 \quad (25)$$

Expressing the solutions as  $A_p = a_p e^{-i\lambda\tau}$ ,  $A_q = a_q e^{-i(\lambda + \sigma)\tau}$  and examining  $\lambda$ , the condition separating bounded and unbounded solutions of Eq. (24) and (25) is

$$\Omega_1 = \frac{1}{s} \left[ \omega_p + \omega_q \pm \varepsilon \sqrt{\frac{(D_{pq}^{(s)})^2 + (E_{pq}^{(s)})^2}{\omega_p\omega_q}} \right] \quad (26)$$

Similarly, the boundaries for instabilities associated with  $s\Omega_2 = \omega_p + \omega_q + \varepsilon\sigma_2$  are

$$\Omega_2 = \frac{1}{s} \left[ \omega_p + \omega_q \pm \varepsilon \sqrt{\frac{(F_{pq}^{(s)})^2 + (G_{pq}^{(s)})^2}{\omega_p\omega_q}} \right] \quad (27)$$

Use of Eqs. (4) and (19) in (26) and (27) yields

$$\Omega_1 = \frac{\omega_p + \omega_q}{s} \pm \frac{2\varepsilon k_{g1}\delta_{1p}\delta_{1q}}{s^2\pi\sqrt{\omega_p\omega_q}} \sin(s c_1 \pi),$$

$$\Omega_2 = \frac{\omega_p + \omega_q}{s} \pm \frac{2\varepsilon k_{g2}\delta_{2p}\delta_{2q}}{s^2\pi\sqrt{\omega_p\omega_q}} \sin(s c_2 \pi) \quad (28)$$

The stability regions associated with each mesh frequency depend on the individual contact ratios but are independent of mesh phasing as the two mesh excitations are uncoupled. For primary and combination instabilities ( $s = 1$ ), maximum regions occur when  $c_1 = c_2 = 1.5$  and minimum regions require  $c_1 = c_2 = \{1, 2\}$ . For secondary instabilities ( $s = 2$ ), the maximum and minimum conditions are  $c_1 = c_2 = \{1.25, 1.75\}$  and  $c_1 = c_2 = \{1, 1.5, 2\}$ , respectively. Figure 6(a) shows the instability regions for  $R = 3/5$ . The boundaries associated with  $\Omega_1$  instabilities (near  $2\omega_3, \omega_2 + \omega_3, \omega_1 + \omega_3$ , and  $\omega_3$ ) are determined by Eq. (26). The primary instability associated with  $\Omega_2 = 2\omega_3 + \varepsilon\sigma_2$  occurs at  $\Omega_1 = R\Omega_2 = R(2\omega_3 + \varepsilon\sigma_2)$  in Fig. 6(a).

When  $R = m$  or  $1/m$  for integer  $m$ , the parametric excitations from the two meshes interact. Consider the case with  $R = 1/m$ , where the  $s = m$  instabilities caused by  $\Omega_1$  overlap with the primary instabilities caused by  $\Omega_2$ . Considering instability of the  $p$ -th mode where  $\Omega_1 = 2\omega_p/m + \varepsilon\sigma_1$  and  $\Omega_2 = m\Omega_1 = 2\omega_p + m\varepsilon\sigma_1$ , the terms leading to unbounded response in Eq. (12) vanish for

$$2i\omega_p\partial A_p/\partial\tau + \bar{A}_p[(D_{pp}^{(m)} + F_{pp}^{(1)}) + i(E_{pp}^{(m)} + G_{pp}^{(1)})]e^{im\sigma_1\tau} = 0 \quad (29)$$

Bounded solution of Eq. (29) is ensured for

$$\sigma_1^2 > [(D_{pp}^{(m)} + F_{pp}^{(1)})^2 + (E_{pp}^{(m)} + G_{pp}^{(1)})^2]/(m\omega_p)^2 \quad (30)$$

For example, when  $\Omega_2 = 2\Omega_1$  ( $R = 1/2$ ), the boundaries for  $\Omega_1$  secondary instabilities (overlapping with  $\Omega_2$  primary instabilities) are

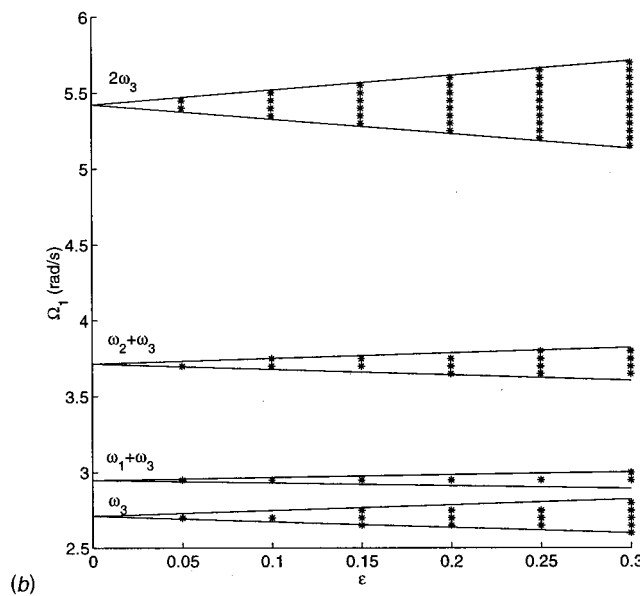
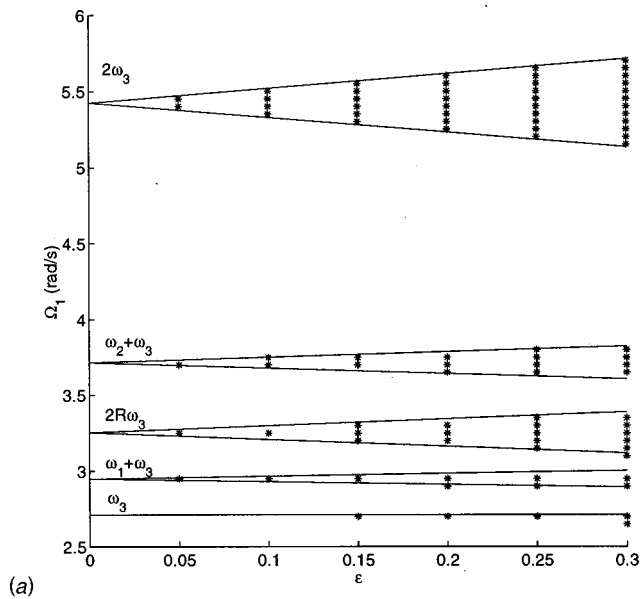
$$\Omega_1 = \omega_p \pm \frac{\varepsilon}{2\omega_p} [(D_{pp}^{(2)} + F_{pp}^{(1)})^2 + (E_{pp}^{(2)} + G_{pp}^{(1)})^2]^{1/2} \quad (31)$$

Figure 6(b) shows instability regions in the  $(\Omega_1, \varepsilon)$  plane for  $R = 1/2$ . Note the instability at  $\Omega_1 \approx \omega_3$  couples with the instability at  $\Omega_2 \approx 2\omega_3$ , and the combined instability region is much larger than the case without interaction [Fig. 6(a)]. Using Eqs. (4) and (19) in (31), the slopes of these boundaries are

$$\sigma_1 = [k_{g1}^2\delta_{1p}^4\sin^2(2c_1\pi) + k_{g2}^2\delta_{2p}^4\sin^2(c_2\pi) + 2k_{g1}k_{g2}\delta_{1p}^2\delta_{2p}^2\sin(2c_1\pi)\sin(c_2\pi) \times \cos(2c_1 - c_2 + 2h)\pi]^{1/2} \frac{2}{\pi\omega_p} \quad (32)$$

Minimization of  $\sigma_1$  requires  $c_1 = \{1, 1.5, 2\}$  and  $c_2 = \{1, 2\}$  for  $1 \leq c_{1,2} \leq 2$ . The instability region can also be reduced by adjusting the phasing  $h$  according to  $\cos(2c_1 - c_2 + 2h)\pi = \pm 1$  with sign the same as  $\sin(2c_1\pi)$ . The primary instability regions under  $\Omega_1$  ( $s = 1$ ) do not coincide with any other instability regions, so these instability boundaries are calculated from Eq. (26) with  $p = q$ . Other overlap situations are possible, such as the  $\Omega_2$  secondary instability ( $s = 2$ ) overlaps with the  $\Omega_1$  fourth instability ( $s = 4$ ), but the interaction between these higher instabilities is typically weak and the instability regions are much smaller. Combination instabilities can be analyzed similarly.

**3.3 Three and Four-Gear Systems: Unequal Mesh Stiffness Variations.** This general case allows all parameters of the two mesh stiffnesses to differ. In contrast with prior cases, the gears may have differing facewidths and material properties such that the amplitudes of stiffness variation at each mesh vary independently ( $\varepsilon_1 \neq \varepsilon_2$ ). The contact ratios and mesh phasing are un-



**Fig. 6** Instabilities regions when  $\Omega_1=R\Omega_2$ ,  $\varepsilon_1=\varepsilon_2=\varepsilon$ . (a)  $R=3/5$ , (b)  $R=1/2$ . The parameters are in Table 1 and  $c_1=c_2=1.5$ ,  $h=0$ .\*\*\* denotes numerical solutions.

restricted. The design of one mesh must account for dynamic interactions with the mesh stiffness variation of the other.

When  $R \neq m$ ,  $1/m$  for integer  $m$ , there is no interaction between the parametric excitations from the two meshes. The  $\Omega_1$  instabilities are only affected by  $\varepsilon_1$  and their boundaries in the  $(\Omega_1, \varepsilon_1)$  plane are  $s\Omega_1 = \omega_p + \omega_q + \varepsilon_1\sigma_1$  with  $\sigma_1$  determined by Eq. (26). The  $\Omega_2$  instabilities are only affected by  $\varepsilon_2$  and their boundaries in the  $(\Omega_2, \varepsilon_2)$  plane are  $s\Omega_2 = \omega_p + \omega_q + \varepsilon_2\sigma_2$  with  $\sigma_2$  determined by Eq. (27).

When  $R = m$  or  $1/m$  for integer  $m$ , a mode may be simultaneously driven to instability by both mesh excitations. In this case, the first mesh instability regions can be significantly affected by the presence of  $\varepsilon_2$  and *vice versa*. Closed-form boundaries of the form (for primary instability)  $\Omega_1 = 2\omega_p + \varepsilon_1\sigma_1 + \varepsilon_2\sigma_2$  for independently varying  $\varepsilon_1$ ,  $\varepsilon_2$  are cumbersome. Alternatively, simple yet accurate approximations for the instability boundaries are ob-

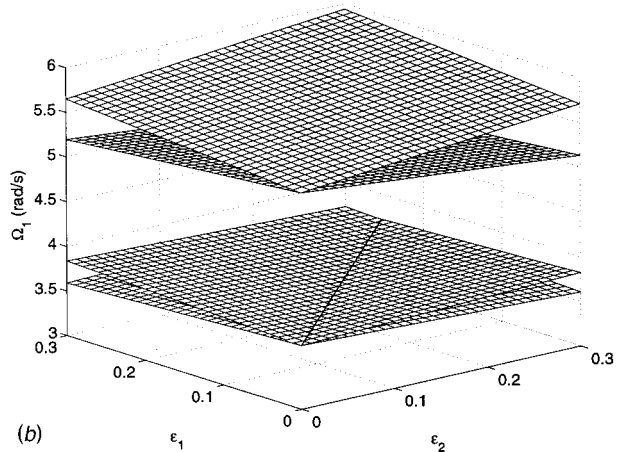
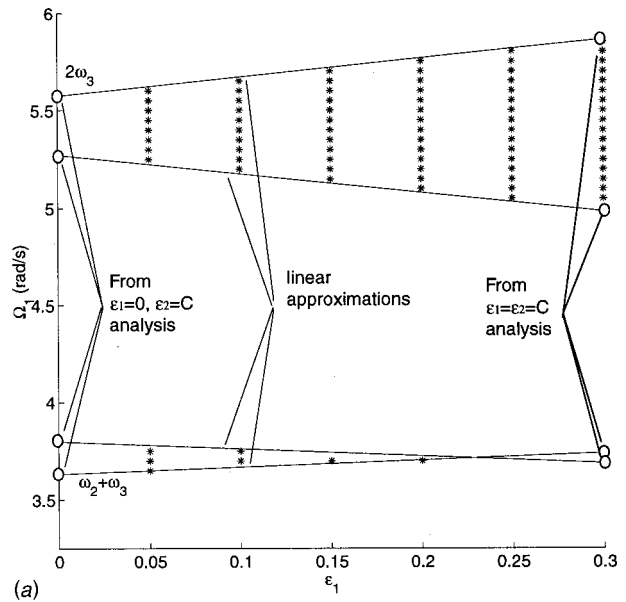


**Fig. 7** Instabilities regions when  $\Omega_1=\Omega_2$ . (a)  $\Omega_1$  versus  $\varepsilon_1$  and  $\varepsilon_2=C=0.3$ . (b)  $\Omega_1$  versus  $\varepsilon_1$ ,  $\varepsilon_2$  and the solid line indicates vanishing of the combination instability. The parameters are in Table 1 and  $c_1=c_2=1.5$ ,  $h=0$ .

tained by presuming a linear variation of the boundaries in the  $(\Omega_1, \varepsilon_1)$  plane for given  $\varepsilon_2$ . To construct this linear approximation, one point is calculated under the condition  $\varepsilon_1=0$ ,  $\varepsilon_2=C$  and a second point is obtained at  $\varepsilon_1=\varepsilon_2=C$ . From Eq. (27), the primary stability boundary limits for  $\varepsilon_1=0$ ,  $\varepsilon_2=C$  are

$$\Omega_1 = 2\omega_p \pm \frac{C}{\omega_p} [(F_{pp}^{(1)})^2 + (G_{pp}^{(1)})^2]^{1/2} \quad (33)$$

From Eq. (18), the stability boundary limits for  $\varepsilon_1=C$ ,  $\varepsilon_2=C$  are

$$\Omega_1 = 2\omega_p \pm \frac{C}{\omega_p} [(D_{pp}^{(1)} + F_{pp}^{(1)})^2 + (E_{pp}^{(1)} + G_{pp}^{(1)})^2]^{1/2} \quad (34)$$

An example is for the primary instability when  $R=1$ ,  $C=0.3$ . Connecting the two points obtained from Eqs. (33) and (34) yields the instability boundaries, which agree well with the numerical solution [Fig. 7(a)]. Assembling the  $(\Omega_1, \varepsilon_1)$  planes for various  $\varepsilon_2=C$  generates three-dimensional plots of  $\Omega_1$  versus  $\varepsilon_1$ ,  $\varepsilon_2$  [Fig. 7(b)]. The parametric excitation in the second mesh dramatically changes the shapes of the instability regions. Notice that the second parametric excitation *widens* the primary instability region for small  $\varepsilon_1$  compared to monofrequency excitation (Fig. 3). In

contrast, the combination instability at  $\Omega_1 \approx \omega_2 + \omega_3$  disappears near  $\varepsilon_1 = 0.23$  in Fig. 7(a). In other words, an otherwise unstable system is stabilized by the presence of a second parametric excitation. The solid line in Fig. 7(b) indicates points where the  $\omega_2 + \omega_3$  combination instability vanishes.

#### 4 An Example

The two-stage gear system [Fig. 1(a)] studied by Tordion and Gauvin [14] and Benton and Seireg [15] is used as an example. These two papers come to markedly different conclusions as discussed below. The system parameters are given in Table 1 and  $c_1 = 1.47$ ,  $c_2 = 1.57$ . In keeping with the published work, the double-tooth contact mesh stiffness  $k_{\max} = 1$  is kept constant, so the average mesh stiffnesses  $k_{gi}$  decreases as  $k_{ai}$  increases [Fig. 2(b)].

Tordion and Gauvin assumed that  $k_{v1}$  and  $k_{v2}$  have the same amplitude and frequency but different contact ratios and phasing. They applied an infinite determinant method [20] to plot the boundaries of primary and secondary instabilities (dashed lines in Fig. 8). Their results deviate significantly from the numerical solution as a result of analytical errors. In addition, the Fourier expansion they derived for rectangular waveforms (Eqs. (11) and (12) in [14]) is incorrect. Nevertheless, they conclude that "The phase displacement between the meshing stiffnesses has a great influence on the width of the instability regions."

Benton and Seireg [15] considered the same system. They decoupled the equations using the modal transformation and neglected the off-diagonal terms of the transformed time-varying stiffness matrix (that is,  $\Phi^T \mathbf{K}_v(t) \Phi$ ). These treatments reduce Eq. (6) to three uncoupled Mathieu equations. The average value of two contact ratios was used to make the stiffness variations  $k_{v1}$  and  $k_{v2}$  identical. With these approximations, they conclude that the instability regions are independent of the mesh phasing, that is, "the normal mode technique . . . without considering the phase variations . . . provide(s) a relatively simple means of predicting the instability regions with sufficient accuracy for practical purposes." This conflicts directly with Tordion and Gauvin. In fact, the mode uncoupling method does not provide satisfactory results when the mesh phasing is non-zero [Fig. 8(b)].

The perturbation results resolve the discrepancy: Mesh phasing strongly impacts the mesh stiffness variation instabilities. In fact, mesh phasing, along with contact ratios, plays a key role in minimizing instability regions as discussed earlier. The excellent agreement of analytical and numerical stability boundaries confirms this finding (Figs. 3, 6, 7, 8).

To further validate the stability conditions, free responses under nontrivial initial conditions are calculated numerically (Fig. 9) for the parameters at point A of Fig. 8 ( $\Omega = 4.2$ ,  $k_a = \varepsilon = 0.3$ ). For point A in Fig. 8(a), the responses are unstable [Fig. 9(a)], as identified by perturbation and numerical methods. This point, however, is stable according to Tordion and Gauvin [Fig. 8(a)]. When the phasing  $h = 0.4$  at point A [Fig. 8(b)], stable responses occur [Fig. 9(b)]. This is consistent with the perturbation and numerical solutions but conflicts with both Tordion and Gauvin's and Benton and Seireg's results.

#### 5 Discussions

Rectangular waveforms are close approximations of the mesh stiffness in spur gears with involute teeth. For helical gears or spur gears with tooth modification, mesh stiffness deviates from the rectangular shape. Equation (4) is not valid for other functions, but the general Fourier expansion (6) can still be used in matrices **D,E,F,G** to determine the instability boundaries.

If damping is considered, the system stability improves and the instability regions shift to the right in the  $(\Omega, \varepsilon)$  plane [10,13]. Furthermore, damping and nonlinearity (e.g., tooth separation) must be considered to determine the limit cycle amplitude of the dynamic response when operating conditions cause instability. Additional study is needed to quantitatively examine these effects

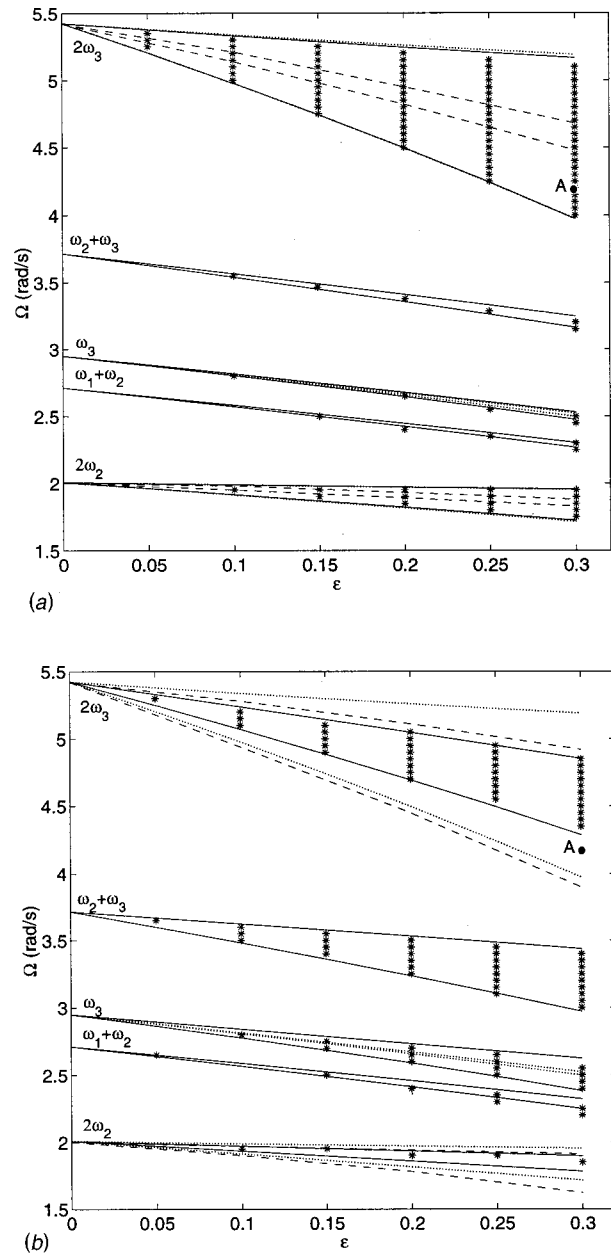


**Fig. 8 Comparison of instability regions from different analyses. The parameters are from Table 1,  $c_1 = 1.47$ ,  $c_2 = 1.57$ , and phasing (a)  $h = 0$ , (b)  $h = 0.4$ . — Perturbation method; \*\*\* Numerical method; --- Tordion and Gauvin (1977); ··· Benton and Seireg (1980).**

in two-stage gear chains. However, the effects of contact ratio and mesh phasing on instability conditions derived in the study are generally applicable to suppress instability and hence contact loss.

The instability analysis can be reduced to single mesh gears with one natural frequency  $\omega_n$ . Setting  $k_{g2} = 0$  in Eqs. (21) and (22), it follows that primary and secondary instabilities vanish as the contact ratio  $c_1 = \{1, 2\}$  and  $c_1 = \{1, 1.5, 2\}$ , respectively. Maximum primary and secondary instability occurs at  $c_1 = 1.5$  and  $c_1 = \{1.25, 1.75\}$ , respectively. Kahraman and Blankenship [16] experimentally studied a pair of spur gears under mesh stiffness excitation for various contact ratios. They showed that the amplitude  $A_1$  in the first mesh frequency harmonic of the response is minimized when the contact ratio  $c_1 = \{1, 2\}$ . This is because parametric excitations are eliminated for integer contact ratios. When the mesh frequency  $\Omega \approx \omega_n$ , their measured  $A_1$  reaches maximum

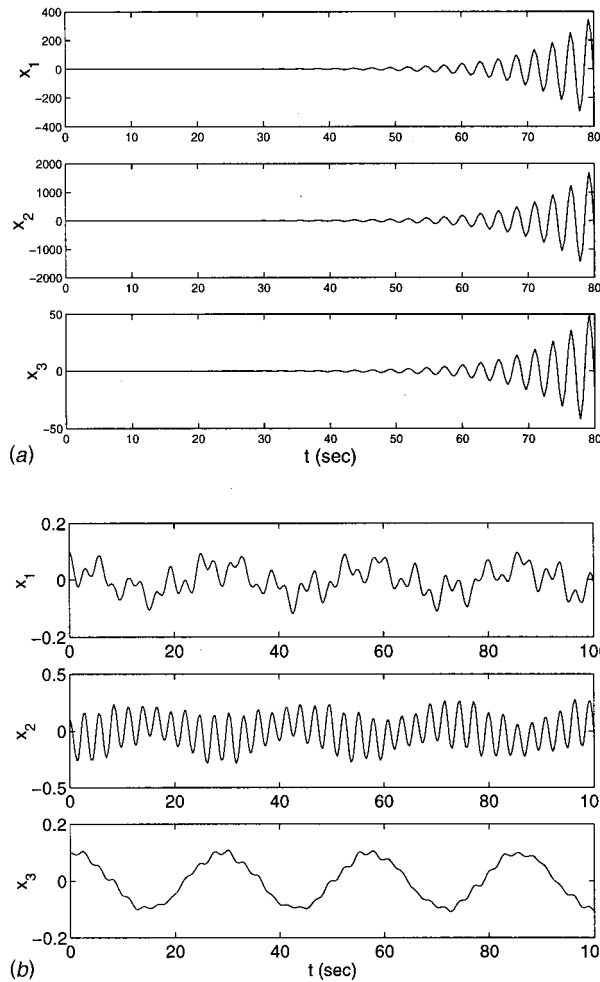


**Fig. 9** Free responses for  $\Omega=4.2$ ,  $k_a=\epsilon=0.3$  (point A in Fig. 8) and the parameters of (a) Fig. 8(a) and (b) Fig. 8(b). The initial conditions are  $x_1=x_2=x_3=0.1$ ,  $\dot{x}_1=\dot{x}_2=\dot{x}_3=0$ .

for  $c_1 \approx 1.4$ . A possible explanation for the high  $A_1$  at this contact ratio is due to the combined effects of primary and secondary instabilities. First, for both primary instability excited by the first harmonic of  $k(t)$  and secondary instability excited by the second harmonic of  $k(t)$ , the dominant response frequency is  $\omega_n$ . The total response at  $\omega_n$  derives from a combination of these components. We now examine the contact ratios where both instabilities are active. Although the maximum primary instability region occurs at  $c_1=1.5$ , the secondary instability region is eliminated there. For  $c_1=\{1.25, 1.75\}$ , the secondary instability region is maximal but the primary instability region is small. For  $c_1 \approx 1.4$  (average of 1.25 and 1.5) or 1.6 (average of 1.75 and 1.5), however, both primary and secondary instabilities have significant instability regions. Generally, the larger an instability region, the higher response amplitude occurs due to this instability (to see this heuristically, note that both the slope of the stability boundaries in Eq. (17) and excitation of first order response in Eq. (10) are proportional to the same quantities **D**, **E**, **F**, and **G**). Accordingly, for  $c_1 \approx 1.4$  and 1.6, both instabilities induce large response and jointly contribute to large  $A_1$ . When the mesh frequency  $\Omega \approx 2\omega_n$ , the instability is caused only by primary instability excited by the first harmonic of  $k(t)$ . Because the primary instability region is maximal at  $c_1=1.5$ , the response amplitude  $A_1$  around  $\Omega \approx 2\omega_n$  also becomes maximal. Therefore, from the viewpoint of dynamic instability and amplitude, contact ratios in the range 1.4~1.6 are harmful to single-mesh gears at high speeds.

## 6 Conclusions

This work analytically investigates the parametric instabilities from mesh stiffness variation in multi-mesh, two-stage gear trains. The effects of mesh stiffness parameters on instabilities are systematically examined. The analysis can be extended to more complicated multi-mesh systems such as planetary gears [21]. The main points are:

- 1 The contact ratios and mesh phasing significantly impact the parametric instabilities. For varying mesh stiffnesses in rectangular waveforms, the conditions for minimum and maximum instability regions are analytically determined in simple, closed forms. Adjusting the contact ratios and mesh phasing is a powerful way to eliminate or reduce the size of parametric instability regions.
- 2 Parametric instabilities in two-mesh gear systems are more complicated than those for single-mesh systems. The excitations from the two meshes interact when one mesh frequency is an integer multiple of the other and dramatically change the instability conditions compared to each excitation acting individually.
- 3 Perturbation and numerical methods provide consistent results that clarify previous, conflicting studies on instability boundaries. Moreover, combination instabilities are examined; these have not been considered previously for geared systems.

## Acknowledgment

The authors thank Timothy L. Krantz of the Army Research Lab at NASA Lewis Research Center for his support and advice on the project. This material is based upon work supported by the NASA Glenn Research Center under grant NAG-1979 and the U.S. Army Research Office under grant DAAD19-99-1-0218.

## References

- [1] Benton, M., and Seireg, A., 1978, "Simulation of Resonances and Instability Conditions in Pinion-Gear Systems," *ASME J. Mech. Des.*, **100**, pp. 26–30.
- [2] Kahraman, A., and Blankenship, G. W., 1997, "Experiments on Nonlinear Dynamic Behavior of an Oscillator with Clearance and Periodically Time-Varying Parameters," *ASME J. Appl. Mech.*, **64**, pp. 217–226.
- [3] Kahraman, A., and Singh, R., 1991, "Interactions Between Time-varying Mesh Stiffness and Clearance Non-linearities in a Geared System," *J. Sound Vib.*, **146**, pp. 135–156.
- [4] Blankenship, G. W., and Kahraman, A., 1995, "Steady State Forced Response of a Mechanical Oscillator with Combined Parametric Excitation and Clearance Type Non-linearity," *J. Sound Vib.*, **185**, pp. 743–765.
- [5] Kahraman, A., and Blankenship, G. W., 1996, "Interactions Between Commensurate Parametric and Forcing Excitations in a System with Clearance," *J. Sound Vib.*, **194**, pp. 317–336.
- [6] Parker, R. G., Vijayaraj, S. M., and Imajo, T., 2000, "Nonlinear Dynamic Response of a Spur Gear Pair: Modeling and Experimental Comparisons," *J. Sound Vib.*, **236**, pp. 561–573.
- [7] Ibrahim, R. A., and Barr, A. D. S., 1978, "Parametric Vibration Part-I: Mechanics of Linear Problems," *Shock Vib. Dig.*, **10**, pp. 15–29.
- [8] Nayfeh, A. H., and Mook, D. T., 1979, *Nonlinear Oscillations*, John Wiley, New York.
- [9] Bollinger, J. G., and Harker, R. J., 1967, "Instability Potential of High Speed Gearing," *J. of Industrial Mathematics*, **17**, pp. 39–55.
- [10] Benton, M., and Seireg, A., 1981, "Factors Influencing Instability and Resonances in Geared Systems," *ASME J. Mech. Des.*, **103**, pp. 372–378.
- [11] Nataraj, C., and Whitman, A. M., 1997, "Parameter Excitation Effects in Gear Dynamics," *ASME Design Engineering Technical Conferences*, Paper No. DETC97/VIB-4018, Sacramento, CA.
- [12] Nataraj, C., and Arakere, N. K., 1999, "Dynamic Response and Stability of a Spur Gear Pair," *ASME Design Engineering Technical Conferences*, Paper No. DETC99/VIB-8110, Las Vegas, NV.
- [13] Amabili, M., and Rivola, A., 1997, "Dynamic Analysis of Spur Gear Pairs: Steady-State Response and Stability of the SDOF Model With Time-Varying

- Meshing Damping,” *Mech. Syst. Signal Process.*, **11**, pp. 375–390.
- [14] Tordion, G. V., and Gauvin, R., 1977, “Dynamic Stability of a Two-Stage Gear Train Under the Influence of Variable Meshing Stiffnesses,” *ASME J. Eng. Ind.*, **99**, pp. 785–791.
- [15] Benton, M., and Seireg, A., 1980, “Normal Mode Uncoupling of Systems with Time Varying Stiffness,” *ASME J. Mech. Des.*, **102**, pp. 379–383.
- [16] Kahraman, A., and Blankenship, G. W., 1999, “Effect of Involute Contact Ratio on Spur Gear Dynamics,” *ASME J. Mech. Des.*, **121**, pp. 112–118.
- [17] Hsu, C. S., 1963, “On the Parametric Excitation of a Dynamic System Having Multiple Degrees of Freedom,” *ASME J. Appl. Mech.*, **30**, pp. 367–372.
- [18] Hsu, C. S., 1965, “Further Results on Parametric Excitation of a Dynamic System,” *ASME J. Appl. Mech.*, **32**, pp. 373–377.
- [19] Friedmann, P. P., 1986, “Numerical Methods for Determining the Stability and Response of Periodic Systems with Applications to Helicopter Rotor Dynamics and Aeroelasticity,” *Comput. Math. Appl.*, **12**, pp. 131–148.
- [20] Bolotin, V. V., 1964, *The Dynamic Stability of Elastic Systems*, San Francisco, Holden-Day Inc.
- [21] Lin, J., and Parker, R. G., 2002, “Planetary Gear Parametric Instability Caused by Mesh Stiffness Variation,” *J. Sound Vib.*, **249**, pp. 129–145.